Applied Catalysis B: Environmental 158–159 (2014) 190–201

Contents lists available at ScienceDirect

Applied Catalysis B: Environmental

journal homepage: www.elsevier.com/locate/apcatb

Synthesis, characterisation and performance evaluation of spinel-derived Ni/Al_2O_3 catalysts for various methane reforming reactions

Zouhair Boukha, Cristina Jiménez-González, Beatriz de Rivas, Juan Ramón González-Velasco, Jose Ignacio Gutiérrez-Ortiz, Rubén López-Fonseca*

Chemical Technologies for Environmental Sustainability Group, Department of Chemical Engineering, Faculty of Science and Technology, University of The Basque Country UPV/EHU, P.O. Box 644, E-48080 Bilbao, Spain

ARTICLE INFO

Article history:
Received 24 January 2014
Received in revised form 4 April 2014
Accepted 7 April 2014
Available online 18 April 2014

Keywords:
Nickel aluminate
Co-precipitation
Co-dissolution
Ni crystallite size
Methane reforming

ABSTRACT

The catalytic performance of bulk nickel aluminate catalysts synthesised by co-precipitation ($NiAl_2O_4$-CP) and co-dissolution ($NiAl_2O_4$-D) was examined for various methane reforming reactions, namely partial oxidation, steam reforming and oxidative steam reforming. The calcined and reduced spinels were thoroughly characterised by a wide number of analytical techniques including *WDXRF*, N_2 physisorption, XRD, UV–visible–NIR DRS, XPS, TEM, H_2-TPR and NH_3-TPD. The characterisation results of the calcined samples at 850 °C showed that nickel aluminate phase was mainly obtained on the $NiAl_2O_4$-CP near-surface together with a small NiO excess. By contrast, a large amount of NiO phase was formed on $NiAl_2O_4$-D and deposited on the spinel surface. The reduction at 850 °C of the two samples produced monodispersed Ni particles (10.6 nm) in the $NiAl_2O_4$-CP while larger metallic nickel (17.7 nm) was deposited on the $NiAl_2O_4$-D. In the three investigated reforming reactions the $NiAl_2O_4$-CP catalyst proved to be highly active, stable and resistant toward carbon deposition. Moreover, the performances of the $NiAl_2O_4$-CP catalyst appeared to be generally comparable with that of a commercial $1\%Rh/Al_2O_3$ catalyst. The difference in catalytic behaviour between the two nickel aluminates was related to the Ni dispersion, its particle size and its capacity to minimise the acid character of the alumina by covering a large part of its surface.

1. Introduction

Methane steam reforming (SRM) is the most used technology for producing synthesis gas (CO and H_2) from natural gas [1–5]. Moreover, this technology is a preferable choice for producing clean and larger hydrogen yield. However, because of the high cost of the endothermic character of SRM, the exothermic methane partial oxidation (POM) appears as an alternative as it offers some interesting advantages especially when the posterior use of the syngas stream requires a suitable H_2/CO ratio [6–8]. Currently industrial facilities are equipped with systems that offer the possibility of using POM and/or SRM technologies. The combination of the POM and SRM strategies called oxidative steam reforming (OSRM) has the advantage of controlling the process heat and the distribution of the products by adjusting the O/C molar ratio [9,10].

Ni-based catalysts are widely used for methane reforming reactions due to their high activity and their competitive costs compared to noble metals [11–13]. Alumina supported Ni systems have particularly received considerable attention because of their practical applications for a variety of reforming reactions [14–18]. Nevertheless, despite exhibiting advantageous catalytic properties, alumina lacks an adequate thermal stability which provokes the sintering of supported metals. Furthermore, the use of alumina as support material has the drawback of rapid deactivation of the catalyst due to carbon deposition on its active acid surface [19,20]. For this reason, the interest of recent investigations has been focused on the preparation of formulations leading to a high dispersion of Ni species which can cover alumina surface, thus minimising the negative effect of its acid character. In this sense, the effect of the addition of some alkali and alkali earth metals, used as chemical promoters, on the activity and stability of Ni/alumina catalysts has been extensively investigated. Typically these additives help to avoid carbon deposition and enhance their stability but at the expense of a reduction of their activity due to the blocking of the more reactive Ni sites [21,22].

* Corresponding author. Tel.: +34 94 6015985; fax: +34 94 6015963.
E-mail address: ruben.lopez@ehu.es (R. López-Fonseca).

http://dx.doi.org/10.1016/j.apcatb.2014.04.014
0926-3373/

Within the same objective (the need to improve stability of Ni-based catalysts) nickel aluminate synthesis is one of the routes proposed in the literature for the design of a precursor capable to produce, after its reduction, metallic Ni presenting strong interaction with alumina [14,15,23–25]. For so long, Ross et al. [25] had evidenced the participation of the reduced surface nickel aluminate sites in the steam reforming of methane over Ni/alumina catalysts. Since then, a number of studies dealing with the preparation of nickel aluminate as precursor of active Ni metallic particles for methane reforming reactions are available in the literature. A great majority of these works have been devoted to the investigation of the influence of preparation methods on the stability and the activity of the final formed Ni structures in reforming reactions [14,15,24,26,27]. As stated in various references, it is however complicated to synthesise pure or stoichiometric nickel aluminate by means of conventional methods of synthesis. This is because of the formation of NiO as an excess even when heating at very high temperatures (>1300 °C) [28–30]. Therefore, many works have examined the impact of this particularity on the catalysts performance [15,16,24,27,31].

In our previous study, we compared two series of Ni/Al_2O_3 catalysts with similar metal content prepared by co-impregnation, using solutions containing a mixture of nickel acetate and aluminium nitrate to obtain a stoichiometric $NiAl_2O_4$ supported on alumina, and simple impregnation of nickel on alumina [15]. We demonstrated that, in methane steam reforming, the co-impregnated catalyst was more active and we attributed this behaviour to its higher Ni–support interaction. We also noticed that obtaining the active metallic Ni, with small particle size, was controlled by the $NiO/NiAl_2O_4$ ratio initially present in the calcined samples. Achouri et al. [16] also studied the influence of the preparation method on the catalytic activity in diesel steam reforming of two alumina-supported nickel aluminate catalysts prepared by wet-impregnation and co-precipitation. They concluded that the impregnated catalyst exhibited a higher catalytic performance and stability over time than the co-precipitated counterpart. This different behaviour was explained by the higher carbon deposition tendency shown by the co-precipitated sample.

In this paper the influence of the physico-chemical characteristics of two bulk nickel aluminate catalysts, prepared by co-precipitation and co-dissolution methods, on their catalytic behaviour in POM, SRM and OSRM reactions is investigated. To reach this target, an extensive characterisation has been carried out by a wide number on analytical techniques including BET measurements, XRD, XPS, UV–visible–NIR DRS, TEM and H_2-TPR. Likewise, TPD of NH_3, a well-known probe molecule for acid sites, has been used to characterise the surface chemistry of the investigated samples. A special attention has been paid to the determination of the different nickel species formed after high-temperature calcination and subsequent high-temperature reduction. In order to examine and compare their catalytic efficiency the two prepared catalysts were evaluated in partial oxidation, steam reforming and oxidative steam reforming of methane. Interesting conclusions are drawn from the correlation between the distribution of Ni active species of the two catalysts and their performance in these three reforming reactions.

2. Experimental

2.1. Catalysts preparation

Bulk nickel aluminate samples were synthesised by co-precipitation (CP) and co-dissolution (D) methods. The sample named $NiAl_2O_4$-D was synthesised using two aqueous solutions of $Ni(CH_3\text{-}COO)_2{\cdot}4H_2O$ and $Al(NO_3)_3{\cdot}9H_2O$. Then they were mixed (leading to a mixture with the desired 1:2 Ni/Al molar ratio), and evaporated on a hot plate (150 °C). In the case of $NiAl_2O_4$-CP, aqueous ammonia was added to the mixed aqueous solutions to adjust the final suitable pH (=8). For comparative purposes NiO was also prepared by simple calcination in air of $Ni(CH_3\text{-}COO)_2{\cdot}4H_2O$. All the samples were dried at 110 °C overnight and then calcined at 850 °C in static air for 4 h at a heating rate of 10 °C min^{-1}. Finally, pellets of bulk (nickel aluminate or nickel oxide) samples were prepared by a process of compressing the powders into flakes in a hydraulic press (Specac), crushing and sieving (0.3–0.5 mm).

2.2. Catalyst characterisation

The catalysts were characterised by N_2 physisorption at −196 °C, wavelength dispersive X-ray fluorescence (WDXRF), X-ray diffraction (XRD), ultraviolet-visible-near infrared diffuse reflectance spectroscopy (DRS), X-ray photoelectron spectroscopy (XPS), temperature programmed reduction with hydrogen (H_2-TPR) and temperature programmed desorption of NH_3 (NH_3-TPD). The experimental details of each analytical technique are described elsewhere [14,15]. Additionally, the morphology and particle size distribution of the nickel particles was examined by transmission electron microscopy (TEM). Prior to analysis, the samples were dispersed in absolute ethanol ultrasonically for 30 min, and 10 cm^3 of each sample were then placed on flexible film (Parafilm® M). Glow-discharged carbon-coated copper grids were inverted onto the droplets of each sample. After incubation for 1 min at room temperature, the grids were manually blotted with filter paper air-dried. Digitally recorded 2D images of each solution were taken at room temperature at a nominal magnification of 80,000 on a Jeol JEM-1230 transmission electron microscope, with a LaB_6 filament as the source of electrons and operated at 100 kV. Digital images were recorded on an Orius SC1000 cooled slow-scan CCD camera, 4008 × 2672 pixels (GATAN), obtaining a final pixel size of 0.85 Å $pixel^{-1}$. The particle size distribution was obtained from the measurement of at least 300 particles using ImageJ software, and the average diameter was calculated by $d_M = \Sigma d_i{\cdot}n_i/\Sigma n_i$, where n_i is the number of the particles of diameter d_i.

On the other hand, the amount of carbonaceous deposits on the used catalyst was determined by dynamic thermogravimetry using a Setaram Setsys Evolution apparatus under atmospheric pressure coupled to a Pfeiffer Prisma mass spectrometer (TPO-MS). The mass loss and the sample temperature were continuously recorded by a computerised data acquisition system. Previously, the samples (20 mg) were dried from room temperature to 150 °C. Then, the temperature was increased from 150 to 850 °C at a constant heating rate of 5 °C min^{-1}. The oxidant stream was 5%O_2/He (50 cm^3 min^{-1}) flowing downwards onto the cylindrical sample holder.

2.3. Catalytic tests

The three methane reforming reactions were studied in a bench-scale fixed-bed reactor operated at atmospheric pressure. The reactor was made of stainless steel with an internal diameter of 9 mm and a height of 305 mm. Prior to the reaction the catalyst (0.125 g) was diluted with inert quartz (0.875 g, 1–1.25 mm). The catalyst bed was maintained in the reactor on a quartz wool plug. The temperature was measured by a thermocouple placed between the particles of the catalyst. Before the reaction the $NiAl_2O_4$-D and $NiAl_2O_4$-CP catalysts were reduced in situ with a mixture of 5%H_2/N_2 at 850 °C for 2 h. Likewise, a 1%Rh/Al_2O_3 (Alfa Aesar, 132 m^2 g^{-1}) commercial catalyst was reduced at 700 °C and its activity was used for comparative purposes in the three methane reforming reactions.

Table 1
Characterisation data of the synthesised nickel aluminate catalysts (calcined, reduced and used in POM, SRM and OSRM reactions).

Samples		Ni (wt.%)[a]	S_{BET} ($m^2\ g^{-1}$)	V_p ($cm^3\ g^{-1}$)	dp (nm	Ni^0 size (nm)[b]	Ni^0 size (nm)[c]	μmol $NH_3\ g^{-1}$[d]	μmol $NH_3\ m^{-2}$[d]
Alumina			133	0.55	2.4	–		503	3.78
$NiAl_2O_4$-D	Calcined	33	55	0.14	7.5	–	–	272	4.95
	Reduced		48	0.12	8.1	23	17.7	274	5.70
	POM		57	0.12	10.7	35	–	–	–
	SRM		47	0.16	11.2	47	–	–	–
	OSRM		37	0.11	9.4	29	–	–	–
$NiAl_2O_4$-CP	Calcined	33	76	0.35	15.4	–	–	291	3.82
	Reduced		55	0.32	19.2	11	10.6	240	4.38
	POM		64	0.34	18.4	5	–	–	–
	SRM		52	0.33	20.3	11	–	–	–
	OSRM		52	0.32	17.7	7	–	–	–

[a] Determined by WDXRF.
[b] Ni^0 crystallites size determined by XRD.
[c] Ni^0 crystallites size determined by TEM.
[d] Total acidity determined by NH_3-TPD.

Three different feed gas mixtures balanced with N_2 (38,400 cm^3 $CH_4\ g^{-1}\ h^{-1}$) were used in each reforming reaction as follows:

(i) 10% CH_4 and 5% O_2 in POM reaction.
(ii) 10% CH_4 and 30% H_2O in SRM reaction.
(iii) 10% CH_4, 30% H_2O and 5% O_2 in OSRM reaction.

The runs were sequentially carried out by increasing and decreasing the reaction temperature (450 °C–550 °C–650 °C–550 °C–450 °C) with an accumulated time online of about 63 h. Catalytic activity, product yields and stability were recorded during 12.5 h at each reaction temperature. Feed and effluent streams were analysed online by a MicroGC (Agilent 3000) equipped with a TCD detector. Two columns, Molecular Sieve 5A and Plot U, were used in a series/bypass arrangement for the complete separation of H_2, N_2, O_2, CH_4, CO and CO_2. A cold trap at the outlet of the reactor was used to condense out any water from the product gas stream. On basis of the molar flow at the inlet and outlet of the reactor, conversion and product yields were calculated, according to the following equations:

$$X(CH_4)(\%) = \frac{F(CO_{out}) + F(CO_{2out})}{F(CH_{4in})} \times 100 \quad (1)$$

$$Y(H_2) = \frac{F(H_{2out})}{2 \cdot F(CH_{4in})} \quad (2)$$

$$Y(CO) = \frac{F(CO_{out})}{F(CH_{4in})} \quad (3)$$

$$Y(CO_2) = \frac{F(CO_{2out})}{F(CH_{4in})} \quad (4)$$

The thermodynamic data were calculated via the HSC Chemistry software package by the GIBBS program using the so-called Gibbs Energy Minimisation Method. For these calculations, only enthalpy, entropy and heat capacity data for all prevailing compounds were needed. The software calculated the amounts of products at equilibrium under isothermal and isobaric conditions. The substances to be taken into account in the calculations, the amount of reactants, the potentially stable phases as well as the temperature of raw species were specified as input. In addition to solid carbon, the following substances in the gas phase were considered: CH_4, O_2, N_2, CO, CO_2, H_2 and H_2O. Calculations were performed in the 450–650 °C temperature range at atmospheric pressure. Hence, the GIBBS program found the most stable phase combination and determined the phase composition where the Gibbs energy for the system reached its minimum at constant pressure and temperature.

3. Results and discussions

3.1. Characterisation of the samples

3.1.1. N_2-physorption (BET measurements)

N_2 adsorption at −196 °C on $NiAl_2O_4$-D and $NiAl_2O_4$-CP showed that the isotherms (not shown) were characteristic of mesoporous solids of type IV according to the IUPAC classification. In the case of $NiAl_2O_4$-D the nitrogen desorption gave rise to a hysteresis loop, H2 type, which was characteristic of disordered porous materials. Table 1 lists the data obtained from the analysis of the textural properties of the calcined and reduced samples. The prepared $NiAl_2O_4$-CP spinel (76 $m^2\ g^{-1}$) had a higher surface area than $NiAl_2O_4$-D (55 $m^2\ g^{-1}$). This difference probably resulted from the preparation method and the corresponding proportion of NiO formed in each sample, which will be discussed in the XRD, H_2-TPR and XPS sections. Fig. 1 shows the pore sizes distribution for the $NiAl_2O_4$-D and $NiAl_2O_4$-CP catalysts. The pore size distribution trace for the $NiAl_2O_4$-D sample exhibited one maximum at 7 nm in the low mesoporous range (<10 nm) whereas the $NiAl_2O_4$-CP samples exhibited a peak centred at 20 nm. After reduction at high temperature (850 °C) both samples decreased their total surface area (48 $m^2\ g^{-1}$ for $NiAl_2O_4$–D and 55 $m^2\ g^{-1}$ for $NiAl_2O_4$-CP); however it did not influence considerably their pore

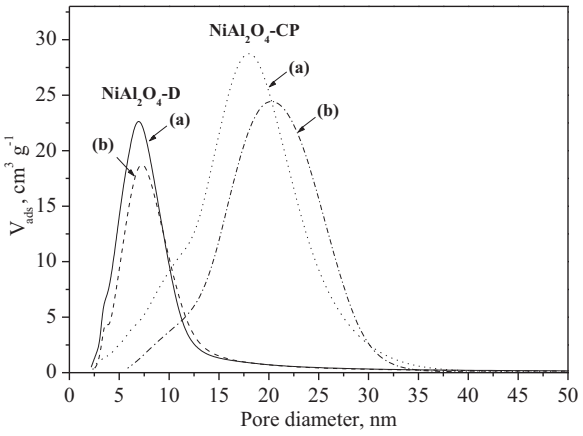

Fig. 1. Mesoporous size distribution for (a) calcined and (b) reduced $NiAl_2O_4$-D and $NiAl_2O_4$-CP catalysts.

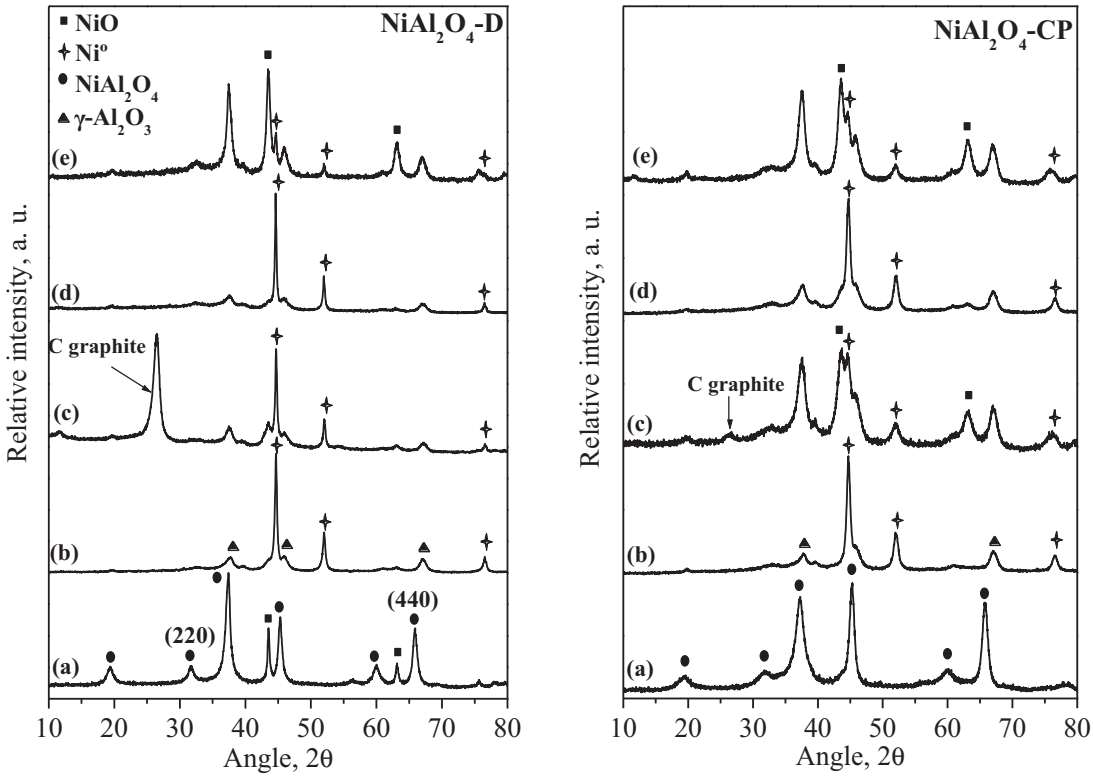

Fig. 2. XRD patterns of $NiAl_2O_4$-D and $NiAl_2O_4$-CP catalysts: (a) calcined, (b) reduced, and tested in (c) POM, (d) SRM and (e) OSRM reactions.

size distribution. A similar observation in line with the decrease of specific surface area by the reduction process was previously reported in various works dealing with Ni/Al_2O_3 catalysts and multiple explanations have been given to describe its origin [23,32]. For instance, Bartholomew et al. [32] reported that the phase transformations and/or dispersed nickel can accelerate the loss of alumina surface area in Ni/Al_2O_3 catalysts.

3.1.2. X-ray diffraction (XRD)

The general formula of stoichiometric nickel aluminates (spinel structure) is $NiAl_2O_4$. It crystallises in the cubic system and belongs to Fd-3 m space group [33–37]. Typically, the framework of the "normal" spinel structures consists of an ensemble of tetrahedral and octahedral coordination occupied by bivalent (Ni^{2+}) and trivalent (Al^{3+}) cations, respectively [33,34]. However, this distribution can change when the Ni^{2+} partially adopts the octahedral site while the tetrahedral site hosts the Al^{3+} together with Ni^{2+} ions. This structural flexibility generates a family of compounds of inverse spinel structure described as $Ni_{1-x}Al_x[Ni_xAl_{2-x}]O_4$ ($0 < x < 1$) [33–37].

The $NiAl_2O_4$-D and $NiAl_2O_4$-CP samples were characterised by means of X-ray powder diffraction in order to investigate their structural properties. Fig. 2 compares the diffractograms of the catalysts before and after reduction at 850 °C. The patterns of the calcined $NiAl_2O_4$-D and $NiAl_2O_4$-CP revealed the formation of the spinel structure (JCPDS 78-1601). Furthermore, in the case of $NiAl_2O_4$-D catalyst additional peaks associated with NiO structure, at 43.5° and 63.1°, were observed whereas the diffractogram of $NiAl_2O_4$-CP showed no lines of NiO. A more careful analysis of the pattern of $NiAl_2O_4$-D evidenced that the intensity ratio of the peaks corresponding to (2 2 0) and (4 4 0) reticular planes differed from that of $NiAl_2O_4$-CP. This difference could be explained by the cation distribution in the octahedral and tetrahedral sites affecting the inversion degree of the spinel structure. The diffraction lines associated with the (2 2 0) plane are related to the tetrahedrally-coordinated cations while the diffraction signals belonging to the (4 4 0) plane are attributed to both tetrahedrally and octahedrally-coordinated cations [35–37]. From our experimental data $I(2\,2\,0)/I(4\,4\,0)$ ratios were estimated. For the $NiAl_2O_4$-CP catalyst this ratio was 0.22, whereas it increased up to 0.33 for the $NiAl_2O_4$-D. The increase in $I(2\,2\,0)/I(4\,4\,0)$ ratio was also observed by Wang et al. [36] in XRD patterns of various inverse spinel structures. This feature was assigned to the increasing occupancy of the heavier cations on the tetrahedral sites. We might accordingly conclude that on the $NiAl_2O_4$-D catalyst nickel was preferentially hosted in tetrahedral sites of the inverse spinel whereas nickel tended to occupy the octahedral coordination in the case of $NiAl_2O_4$-CP sample prepared by co-precipitation.

Fig. 2 also includes the X-ray diffraction patterns of the bulk nickel aluminates reduced at 850 °C. A comparison of the $NiAl_2O_4$-CP patterns before and after reduction confirmed that the transformation of Ni^{2+} ions of the spinel framework into metallic Ni (JCPDS 89-7128) was complete. Likewise, the formation of alumina structure (JCPDS 79-1558) instead of the characteristic peaks attributed to spinel structure was noted. However, in the case of the $NiAl_2O_4$-D sample, diffraction peaks with a low intensity attributed to NiO were also observed. This could be reasonably explained by the surface room temperature passivation of the catalyst [31]. Table 1 reports the metallic Ni crystallite size, calculated by Scherrer equation, by using Ni (2 0 0) ($2\theta = 51.6°$) diffraction line broadening. The average size of Ni particles was found to be around 11 nm on the reduced $NiAl_2O_4$-CP while larger particles with an average size of about 23 nm were detected for the reduced $NiAl_2O_4$-D.

In sum, the obtained XRD results indicated that the preparation method of nickel aluminate had an important effect on the excess of NiO and the Ni^{2+} ions distribution, between tetrahedral and octahedral sites in the spinel structure. Moreover, the reduction of the $NiAl_2O_4$-CP sample prepared by co-precipitation method produced smaller Ni particles in comparison with the $NiAl_2O_4$-D catalyst.

Table 2
Results from H_2-TPR and XPS studies of the calcined $NiAl_2O_4$-D and $NiAl_2O_4$-CP samples.

Catalyst	H_2-TPR					XPS				
	Theoretical H_2 uptake (mmol g^{-1})	Experimental H_2 uptake (mmol g^{-1})	Relative amount of reducible Ni species (%)			Ni/Al	Ni $2p_{3/2}$			O 1s
			α^*	β^{**}	γ^{***}		Peak (eV)	Ni (% in the sites)	Satellite (eV)	Peak (eV)
$NiAl_2O_4$-D	5.7	5.8±0.1	33	18	49	1	854.1(1); 856.8(2)	61.7(1);38.3(2)	861.3	528.5 (a); 531.1 (b); 532.6 (c)
$NiAl_2O_4$-CP	5.7	5.6±0.1	9	47	44	0.6	855.7 (2)	100(2)	861.8	530.6 (b)

(*) Reduction peak of NiO excess.
(**) and (***) reduction peaks of Ni^{2+} in nickel aluminate.
(1) Ni^{2+} as NiO and (2) Ni^{2+} as $NiAl_2O_4$.
(a) O^{2-} as NiO, (b) O^{2-} as $NiAl_2O_4$ and (c) O^{2-} as Al_2O_3.

3.2. Temperature programmed reduction (H_2-TPR)

The TPR experiments were performed in order to determine the different Ni reducible species present in the two prepared spinel catalysts (Fig. 3). The H_2-TPR profiles included in Fig. 3 suggested the full reduction of the spinel catalysts ($NiAl_2O_4$-D and $NiAl_2O_4$-CP) with an overall H_2 uptake close to the theoretical value 5.7 mmol H_2 g^{-1} (within the experimental error) (Table 2). It was observed, however, that the shape of the TPR traces depended on the preparation method. The thermogram of the $NiAl_2O_4$-D sample displayed a typical reduction spectrum of a mixture of two Ni species consisting of free NiO (α-peak at 400 °C) and nickel aluminates structures (β-peak at 600 °C and γ-peak at 800 °C) [14,15]. In the case of $NiAl_2O_4$-CP catalyst it was noted that the characteristic reduction peak attributed to bulk NiO (at 400 °C) was absent. The observed three H_2 uptakes in the profile of the $NiAl_2O_4$-CP catalyst were located at 520, 750 and 825 °C. The peak at 520 °C was attributed to the highly dispersed NiO. Generally, the NiO reduction peak shifts towards high temperatures, as in the case of $NiAl_2O_4$-CP catalyst, when the NiO particles strongly interact with the support

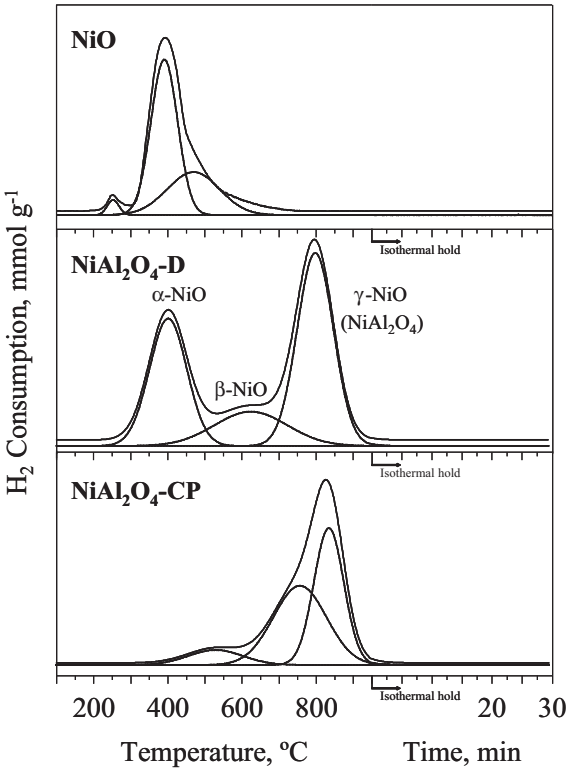

Fig. 3. H_2-TPR profiles of $NiAl_2O_4$-D and $NiAl_2O_4$-CP catalysts.

[31]. Above 600 °C, the high-temperature reduction peaks at 750 and 825 °C were due to the reduction of Ni^{2+} ions incorporated in the nickel aluminate structure. The relative abundance of the NiO species in the $NiAl_2O_4$-D and $NiAl_2O_4$-CP samples was estimated to be 33% and 9%, respectively (Table 2). Since the specific surface area of the bulk NiO was very low (≤1 m^2 g^{-1}), the relative abundance of the NiO in each sample could explain the difference observed in the specific surface area. Note that the XRD pattern of the $NiAl_2O_4$-CP catalyst showed that no peaks due to NiO were observed probably because of its low amount and/or its high dispersion.

Though it was reported that free NiO present on the spinel reduces at low temperature and favours the reduction of nickel located in the spinel [24], to our knowledge, the real origin of the splitting of the nickel aluminates peak reduction has never been discussed. As deduced from our XRD study, on the $NiAl_2O_4$-D catalyst, nickel mainly has a tetrahedral coordination whereas it was mainly octahedrally coordinated in the case of $NiAl_2O_4$-CP. We believe that the two observed reduction peaks and their position could be related to the different Ni^{2+} coordination in the spinel framework. Furthermore, since the contribution of the β-peak in the total Ni species present in the spinel structure of $NiAl_2O_4$-D was lower (27%) than that of $NiAl_2O_4$-CP (51%), it could be concluded that Ni^{2+} ions occupying octahedral sites were more prone to be reduced than the tetrahedral ones.

3.3. UV–visible–NIR diffuse reflectance spectroscopy (DRS)

The coordination and the oxidation state of nickel species on the $NiAl_2O_4$-D and $NiAl_2O_4$-CP catalysts were studied by means of diffuse reflectance spectroscopy. Fig. 4 showed the UV-visible-NIR spectra of the two prepared samples and the spectrum of pure NiO presented as reference. The shape of $NiAl_2O_4$-CP and $NiAl_2O_4$-D spectra resulted almost identical. All the spectra displayed a strong absorption in the UV domain. The maxima centred at 220–345 nm were ascribed to $O^{2-} \rightarrow Ni^{2+}$ metal to ligand charge transfers [14,15,38]. In the visible range, the bands located at 380 nm and 720 nm were associated with ν_3 ($^3A_{2g} \rightarrow {}^3T_{1g}$ (P)) and ν_2 ($^3A_{2g} \rightarrow {}^3T_{1g}$) absorptions that resulted from d-d transitions of Ni^{2+} ions hosted by octahedral sites [14,15,38,39]. The spectra were also characterised by the presence of an additional intense band in the range of 600–645 nm and shoulders at 550 nm and 760 nm, assigned to the ($^3T_1$(F) → $^3T_{1g}$ (P)) ligand transitions, thereby evidencing the presence of the tetrahedrally coordinated Ni^{2+} ions.

In the NIR a broad resolved band located around 1130 nm was observed which was ascribed to the ν_1 ($^3A_{2g} \rightarrow {}^3T_{2g}$) transition of Ni^{2+} in octahedral symmetry [14,15,38,39]. Comparing the intensity of this absorption band it was clear that the relative abundance of octahedral Ni^{2+} ions in $NiAl_2O_4$-CP was superior to that of $NiAl_2O_4$-D. This was in accordance with the results obtained by XRD. However, the quantification of tetrahedral Ni^{2+} ions on the

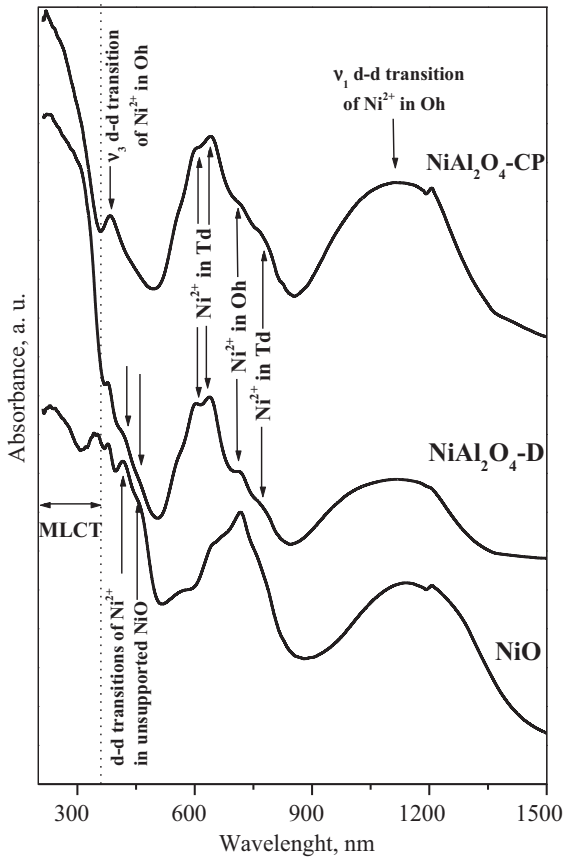

Fig. 4. UV–vis–NIR spectra of $NiAl_2O_4$-D and $NiAl_2O_4$-CP catalysts.

spectra was difficult because of the overlapping of the absorption domains of Ni^{2+} ions in tetrahedral and octahedral symmetries.

On the other hand, it should be pointed out that the spectrum of $NiAl_2O_4$-D exhibited two additional shoulders: (i) the first one was located around 420 nm, (ii) the second one at a wavelength of 450 nm. Since the presence of these bands was also detected in the spectrum of NiO, they could be assigned to d–d transitions caused by the ligand field of unsupported NiO. These bands were expectedly absent from the spectrum of $NiAl_2O_4$-CP, thus confirming that NiO was exclusively formed on the calcined $NiAl_2O_4$-D. These results suggested, in line with XRD characterisation, that in contrast to $NiAl_2O_4$-CP, the preparation of $NiAl_2O_4$-D led to the formation of nickel aluminate together with NiO structure. Furthermore, these evidences could reasonably explain the greenish-blue colour of the $NiAl_2O_4$-D sample and the dark blue colour of $NiAl_2O_4$-CP.

3.4. X-ray photoelectron spectroscopy (XPS)

The chemical composition and the distribution of nickel species laying on the surface of the calcined $NiAl_2O_4$-CP and $NiAl_2O_4$-D catalysts were investigated by means of XPS measurements. The Ni $2p_{3/2}$ and O 1s photoemission peaks for the two analysed samples were shown in Fig. 5. The different broadness and the symmetry of the Ni $2p_{3/2}$ and O 1s main peaks for $NiAl_2O_4$-CP and $NiAl_2O_4$-D oxides were evident. As revealed by the analysis of the spectra included in Fig. 5 the $NiAl_2O_4$-D sample showed much broader and less symmetric peaks, thus suggesting a larger heterogeneity in its nickel environments. On the basis of these observations the Ni $2p_{3/2}$ and O 1s spectra of $NiAl_2O_4$-D were deconvoluted. As a result, the main Ni $2p_{3/2}$ XPS peak displayed two bands. The first one located at 854.1 eV was associated with NiO exhibiting weak interaction NiO-$NiAl_2O_4$ [15]. The second one, centred at 856.8 eV, was related to Ni^{2+} ions in the network of nickel aluminates [15]. On the other hand, the O 1s signal of the $NiAl_2O_4$-D XPS spectrum could be decomposed into three components: the first one at 528.5 eV assigned to O^{2-} in NiO, the second situated at 531.1 eV due to $NiAl_2O_4$ phase and the third one located at high binding energies 532.6 eV characteristic of pure Al_2O_3 [15]. By contrast, because of their apparent symmetry the O 1s and Ni $2p_{3/2}$ signals of $NiAl_2O_4$-CP catalyst suggested the presence of a unique phase. The comparison of the positions of the O 1s (530.6 eV) and Ni $2p_{3/2}$ (855.7 eV) peaks with the attributions mentioned above revealed that the $NiAl_2O_4$-CP near-surface was mainly composed of nickel aluminate structure. Note that despite of the fact that the occurrence of the small fraction of NiO phase was detected for this sample by H_2-TPR, its XPS spectra did not reveal the presence of this species. This might be explained by the strong interaction of the highly dispersed NiO with $NiAl_2O_4$ phase that was reflected by the shifting of its XPS peak towards higher binding energy.

The difference in Ni/Al atomic ratio determined by XPS between $NiAl_2O_4$-CP and $NiAl_2O_4$-D also supported our conclusion about the structural composition of near-surface. According to Table 2, the Ni/Al atomic ratio of $NiAl_2O_4$-CP (0.6) was smaller than that determined for $NiAl_2O_4$-D (1), suggesting that the surface of the co-precipitated sample was comparatively deficient in nickel. Thus, in view of the stoichiometry of the pure spinel (Ni/Al = 0.5), it could be concluded that nickel aluminate phase was mainly obtained on the

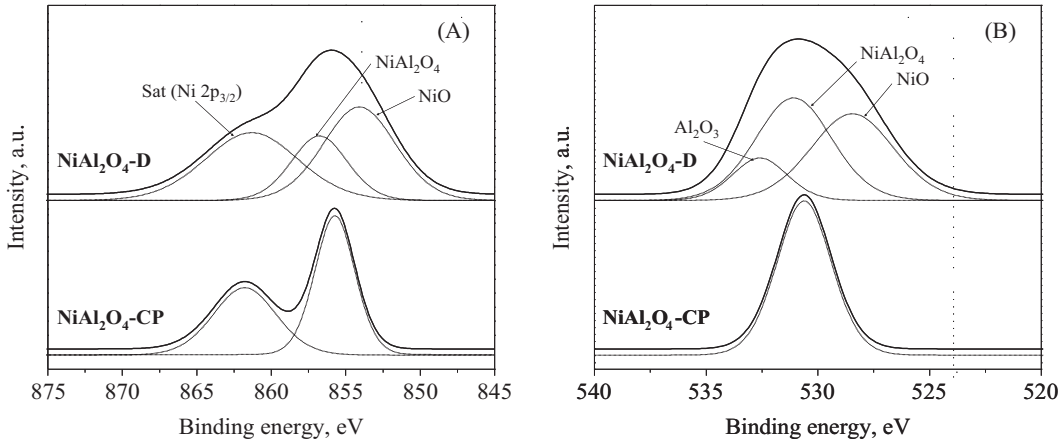

Fig. 5. XPS spectra of Ni $2p_{3/2}$ region (A) and O 1s region (B) of $NiAl_2O_4$-D and $NiAl_2O_4$-CP catalysts.

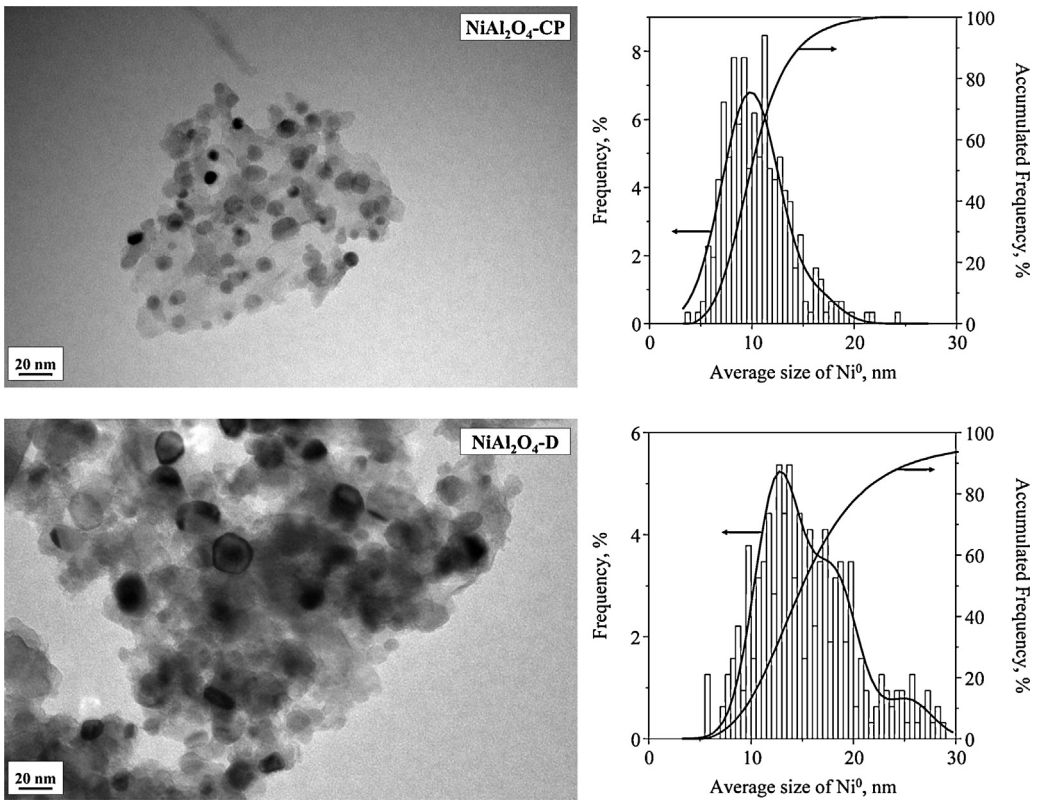

Fig. 6. TEM images and Ni particle size distribution of reduced $NiAl_2O_4$-D and $NiAl_2O_4$-CP catalysts.

$NiAl_2O_4$-CP near-surface together with a small NiO excess. A larger amount of NiO phase was however formed on $NiAl_2O_4$-D.

3.5. Transmission electron microscopy (TEM)

$NiAl_2O_4$-CP and $NiAl_2O_4$-D samples, reduced at 850 °C, were investigated by transmission electron microscopy as well. Fig. 6(a) and (b) shows the TEM micrographs and size distribution diagrams (obtained from the measurement of about 300 particles). The micrographs of both samples showed no significant differences in morphology. In both cases spherical particles of nickel were observed. Nevertheless, it was visualised that nickel was homogeneously dispersed in $NiAl_2O_4$-CP while it was much more heterogeneous on the $NiAl_2O_4$-D catalyst. The particle size distribution in the co-precipitated sample presented a unimodal shape with an average size of 10.6 nm (dispersion of 9.5%). By contrast a broad distribution ranging from 10 to 50 nm was obtained for the $NiAl_2O_4$-D catalyst with a corresponding average size of 17.7 nm (dispersion of 4%). By correlating the Ni particle size distributions with the results of H_2-TPR, XRD, XPS and UV-visible-NIR DRS it could be reasonably assumed that the smaller mono-dispersed particles present on the $NiAl_2O_4$-CP corresponded to particles resulted from the reduction of nickel aluminate phase whereas the range of larger particles deposited on the $NiAl_2O_4$-D was originated by the reduction of the free NiO. As stated previously, the $NiAl_2O_4$-D catalyst contained two Ni species as a mixture of free NiO and nickel aluminate phase while $NiAl_2O_4$-CP was composed mainly by nickel aluminate together with a relatively small fraction of highly dispersed NiO (as proved by H_2-TPR). Furthermore, we thought that the difference between $NiAl_2O_4$-D and $NiAl_2O_4$-CP probably resulted from the textural properties of each catalyst as well. The $NiAl_2O_4$-D average pore size was smaller (7.5 nm) compared to its Ni particles average size, suggesting that nickel was mainly deposited on the external surface. However, the $NiAl_2O_4$-CP average pore size was around 15 nm and this might limit the growth of the Ni crystallites during the reduction.

3.6. Temperature programmed desorption of NH_3 (NH_3-TPD)

The surface acidity of the two catalysts was characterised by means of temperature programmed desorption, using ammonia as probe molecule, followed by dynamic thermogravimetry and coupled to a mass spectrometer [15]. The overall acidity of the samples (calcined and reduced spinel catalysts) was quantified from the net weight gain during the adsorption step at 100 °C followed by the removal of physically bound ammonia from the surface with flowing helium.

The deconvolution of the NH_3-TPD thermograms of the calcined $NiAl_2O_4$-D and $NiAl_2O_4$-CP samples exhibited two bands corresponding to two types of acid sites (Fig. 7). The first one consisted of a peak located at low temperatures (≤220 °C) accompanied by a second much more intense feature at relatively high temperatures (250–370 °C), the latter being probably due to a fraction of strong acid sites present at the surface of the catalysts. It must be pointed out that, in the case of the two reduced samples, the MS analysis of the exit stream revealed the presence of trace amounts of N_2 and H_2 related to the decomposition of the probe molecule on the reduced sites.

The obtained quantitative results were summarised in Table 1. It was found that the surface density of NH_3 adsorbed on the calcined $NiAl_2O_4$-CP, 3.82 μmol NH_3 m^{-2}, was smaller than that determined for the calcined $NiAl_2O_4$-D, 4.95 μmol NH_3 m^{-2}. The difference could be related to the structural composition of each catalyst. As demonstrated by XPS analysis the $NiAl_2O_4$-D catalyst contained alumina phase in its near-surface which could improve its surface acid properties. It should be pointed out that the H_2

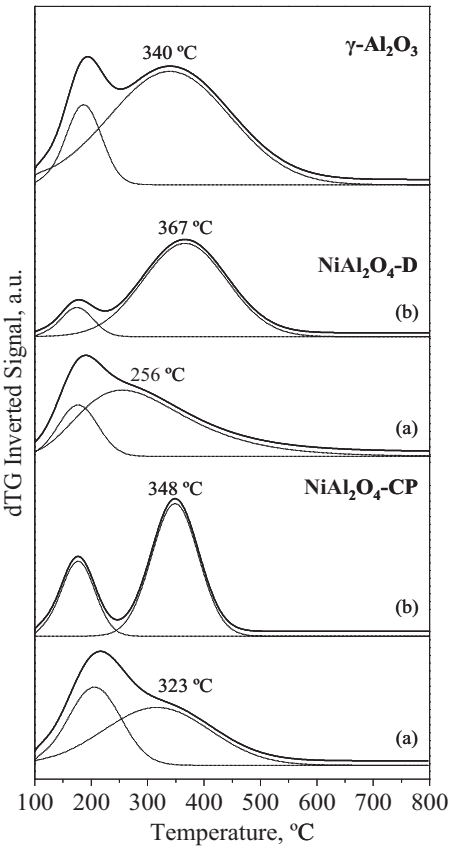

Fig. 7. NH_3-TPD patterns of (a) calcined and (b) reduced $NiAl_2O_4$-D and $NiAl_2O_4$-CP catalysts.

reduction at 850 °C of the two catalysts appeared to increase both the amount and the thermal stability of the adsorbed NH_3 by shifting the desorption peaks towards higher temperatures. The acid surface density for reduced $NiAl_2O_4$-CP was estimated to reach 4.38 μmol NH_3 m^{-2} in comparison with 5.7 μmol NH_3 m^{-2} for $NiAl_2O_4$-D (Table 1). These results might be related to the formation of alumina instead of nickel aluminate structure in the two reduced samples, as proved by XRD analysis. In addition, the presence of homogeneous and highly dispersed nickel in the reduced $NiAl_2O_4$-CP catalyst, as confirmed by TEM analysis, could explain the occurrence of a small fraction of surface acid sites in comparison with $NiAl_2O_4$-D. By contrast, the low Ni dispersion (4%) on the latter led to a large uncovered acid support surface.

3.7. Catalytic activity

3.7.1. Partial oxidation of methane (POM)

The POM reaction was carried out on the activated (calcination followed by reduction) $NiAl_2O_4$-CP, $NiAl_2O_4$-D and 1%Rh/Al_2O_3 (used as reference) catalysts, at 450, 550 and 650 °C, by sequentially increasing the reaction temperature with 100 °C intervals. The inverse sequence was conducted by decreasing the reaction temperature (from 650 to 550 and 450 °C) in order to probe the stability of the catalysts. Fig. 8 shows the obtained results in terms of CH_4 conversion and H_2, CO and CO_2 yields. The corresponding equilibrium data are included as well (calculated via the HSC Chemistry software package by the GIBBS program using the so-called Gibbs Energy Minimisation Method). The reported data evidenced that the $NiAl_2O_4$-CP catalyst was typically more active than the $NiAl_2O_4$-D. Furthermore, over the co-precipitated sample methane conversion as well as H_2, CO and CO_2 yields were fairly stable during 12.5 h on stream (Fig. 9). At 450 °C the conversion on this sample was around 25% and it increased to reach about 36% at 550 °C and 58% at 650 °C. Likewise, the increase in the reaction temperature promoted the H_2 yield, which attained 0.56. Carbon monoxide production also increased up to 0.44 at 650 °C. It is noteworthy that at 650 °C both conversion and yields achieved with $NiAl_2O_4$-CP were close to the values obtained with the commercial 1%Rh/Al_2O_3 catalyst. As the performance of the noble metal-based catalyst is considered as reference in the POM reaction [40–43], these catalytic features evidenced the potential of $NiAl_2O_4$-CP as a promising alternative catalyst. By contrast, the activity appeared to decrease with time on stream in the case of $NiAl_2O_4$-D catalyst. It was thought that this difference in the catalytic activity between the two reduced spinel catalysts was related to the Ni particle size. Indeed, our TEM results showed that on the $NiAl_2O_4$-CP catalyst metallic nickel was deposited with a smaller size (10.6 nm) compared to the $NiAl_2O_4$-D (17.7 nm).

As shown in Fig. 9, methane conversion at 450 °C gradually decreased from 29% at the beginning of the reaction to 25% after 12.5 h on stream. Likewise, H_2, CO and CO_2 yields were not stable with time on line. Indeed, a slight increase in activity followed by a stable plateau was observed when the reaction temperature decreased which could be a result of an excess of carbon formation (Fig. 9).

Table 3 lists the H_2/CO and CO/CO_2 ratios calculated for each reaction temperature on the tested catalysts. Note that, on the two tested nickel catalysts, the CO/CO_2 ratio seemed to increase with reaction temperature. For instance, at 450 °C the CO/CO_2 ratio on the $NiAl_2O_4$-CP was around 0.1 and it increased to reach about 3 at 650 °C. At low CO/CO_2 values (corresponding to relatively low temperatures) CO disproportionation and/or methane total oxidation reaction may occur producing CO_2 and carbon and/or H_2O. On the other hand, the H_2/CO ratio was in all the cases higher than 2 (ranging between 2.2 and 2.5). It is widely accepted that the encapsulation of the metal particles by deposited carbon does not occur if H_2/CO or H_2O/hydrocarbon ratios are sufficiently high [32]. Accordingly, our results showed, by comparing the $NiAl_2O_4$-CP and $NiAl_2O_4$-D catalysts, that the catalyst with the highest H_2/CO ratio ($NiAl_2O_4$-CP) did not suffer apparent deactivation.

Thermogravimetric (not shown) and TPO-MS analyses (Fig. 10) performed in order to determine the amount of carbon accumulated on the used catalysts in POM resulted in deposited carbon masses of 2.4 wt.% on $NiAl_2O_4$-CP (close to 2 wt% observed for the commercial rhodium catalyst) and 46.5 wt.% on $NiAl_2O_4$-D (Table 3). Both TPO traces consisted of a CO_2 production major peak at approximately 670 °C (Fig. 10). Thus, the same type of carbonaceous species was present on the two catalysts. It could be concluded, therefore, that the deactivation of $NiAl_2O_4$-D catalyst might mainly occur as a result of the substantial formation of coke. This was in agreement with XRD analysis of the spent catalysts which confirmed the formation of carbon (graphite) on the two catalysts. Specially, it was observed that the principal peak (26.4°) was much more intense in the $NiAl_2O_4$-D diffractogram than that of $NiAl_2O_4$-CP catalyst (Fig. 2). On the other hand, the Ni (200) ($2\theta = 51.6°$) diffraction line broadening was used to estimate, by Scherrer equation, the evolution of metallic Ni crystallite size after catalytic test (Table 1). It was found that the growth of Ni^0 crystallites during POM reaction on $NiAl_2O_4$-D for extended periods of time was significant (size estimated to be around 23 nm in the reduced sample while it was around 35 nm after catalytic test). In agreement with a previous study which reported that, in the methane reforming reactions, the larger Ni crystallites on the Ni catalyst favoured the formation of graphitic carbon [44], we could conclude that the same phenomenon occurred in the case of our $NiAl_2O_4$-D catalyst. As stated previously, the

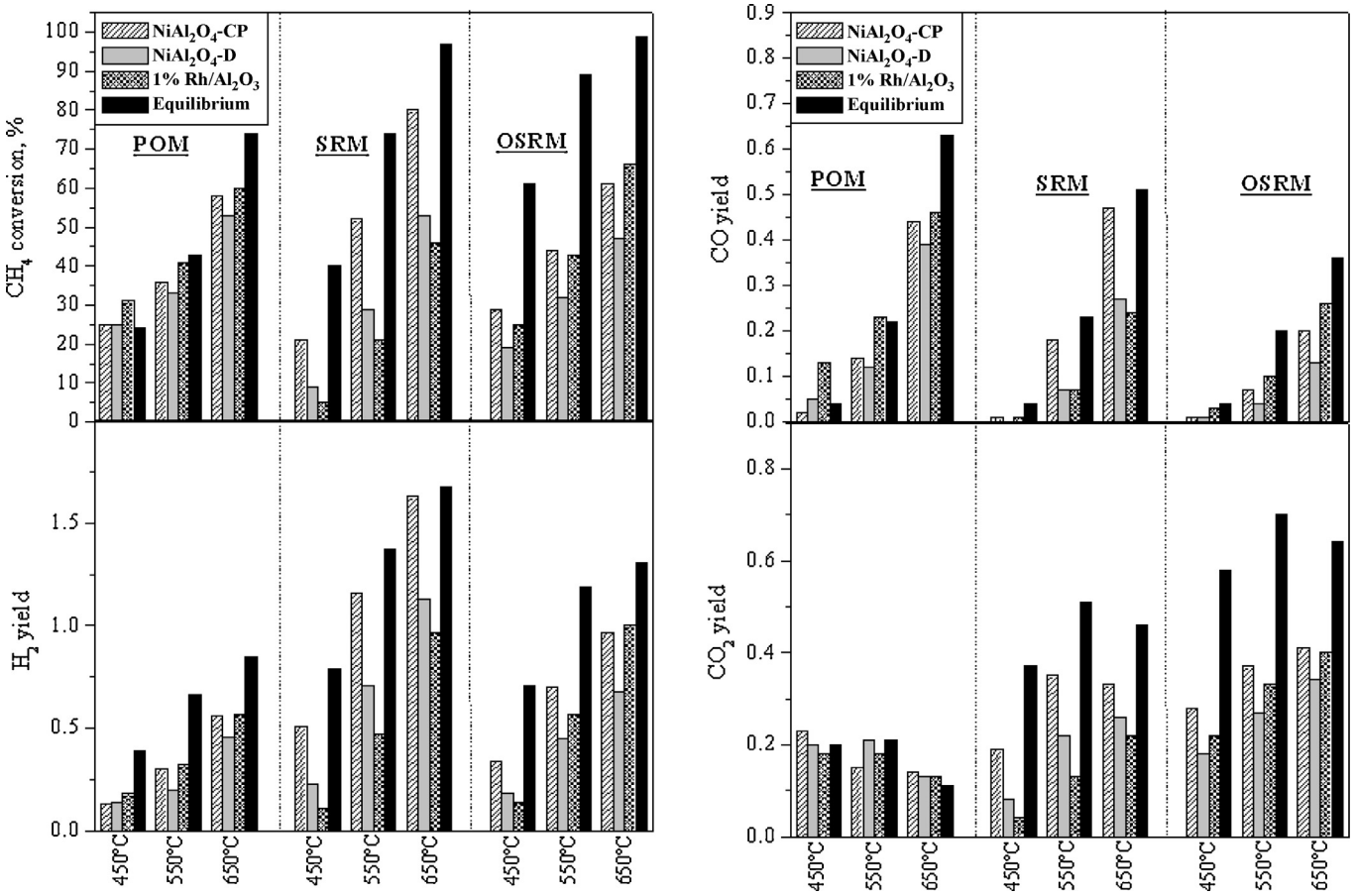

Fig. 8. Methane conversion and H_2, CO and CO_2 yields over reduced $NiAl_2O_4$-CP and $NiAl_2O_4$-D catalysts versus reaction temperature in POM, SRM and OSRM reactions. Reactions conditions: 38,400 cm^3 CH_4 g^{-1} h^{-1}; W = 0.125 g. Gas mixtures: POM: 10%CH_4/5%O_2/N_2, SRM: 10%CH_4/30%H_2O/N_2 and OSRM: 10%CH_4/30%H_2O/5%O_2/N_2. Data corresponding to the commercial 1%Rh/Al_2O_3 catalyst and the thermodynamic equilibrium were also included.

reduction of the Ni species deposited on this sample produced large metallic Ni which was less resistant to sintering and coke formation.

The XRD diffractograms of the spent nickel aluminate catalysts also evidenced the presence of NiO phase (Fig. 2). The NiO characteristic peaks were much more intense on the $NiAl_2O_4$-CP diffractogram suggesting that the oxidation of Ni species during the POM reaction was influenced by their interaction with the support. Accordingly, it seemed that the oxidation of the smaller Ni particles, during POM reaction, might be easier. Indeed, our H_2-TPR and TEM studies indicated that more than two distinct metallic nickel populations were present on $NiAl_2O_4$-D in contrast with the $NiAl_2O_4$-CP catalyst with a narrower and more homogeneous size distribution (size = 10.6 nm). In their study on the mechanism for POM reaction, Jin et al. [45] claimed that during the CH_4/O_2 reaction over Ni/Al_2O_3 catalysts, Ni^0 was first oxidised to NiO, and the latter was reduced again by CH_4 during the transient process. Since the reduction of NiO by CH_4 is endothermic and as the last step of our catalytic experiments occurred at 450 °C (relatively low temperature) the presence of the characteristic peaks of

Table 3
Values for H_2/CO and CO/CO_2 ratios and coke content in POM, SRM and OSRM reactions over $NiAl_2O_4$-D and $NiAl_2O_4$-CP catalysts.

Reaction	Catalyst	H_2/CO			CO/CO_2			Coke (%)[a]
		450 °C	550 °C	650 °C	450 °C	550 °C	650 °C	–
POM	Equilibrium	21.3	6.0	2.7	0.19	1.06	5.86	–
	$NiAl_2O_4$-D	5.5	3.5	2.2	0.24	0.57	3.00	46.5
	$NiAl_2O_4$-CP	12.7	4.4	2.5	0.10	0.60	3.00	2.5
	1%Rh/Al_2O_3	2.5	2.8	2.4	0.74	1.29	3.46	2
SRM	Equilibrium	44.9	11.9	6.7	0.10	0.45	1.09	–
	$NiAl_2O_4$-D	118.6	19.2	8.5	0.05	0.34	1.03	<1
	$NiAl_2O_4$-CP	68.5	13.3	6.9	0.08	0.51	1.42	<1
	1%Rh/Al_2O_3	19.7	12.6	8.2	0.31	0.56	1.06	<1
OSRM	Equilibrium	36.3	12.1	7.3	0.07	0.28	0.56	-
	$NiAl_2O_4$-D	43.1	20.1	10.3	0.05	0.16	0.39	<1
	$NiAl_2O_4$-CP	55.9	20.1	9.4	0.04	0.18	0.50	<1
	1%Rh/Al_2O_3	8.9	10.8	7.8	0.14	0.31	0.65	<1

Reactions conditions: 38,400 cm^3 CH_4 g^{-1} h^{-1}; W = 0.125 g. Gas mixtures: POM: 10%CH_4/5%O_2/N_2, SRM: 10%CH_4/30%H_2O/N_2 and OSRM: 10%CH_4/30%H_2O/5%O_2/N_2.
[a] Deposited carbon for used catalyst determined by TPO and TG analyses.

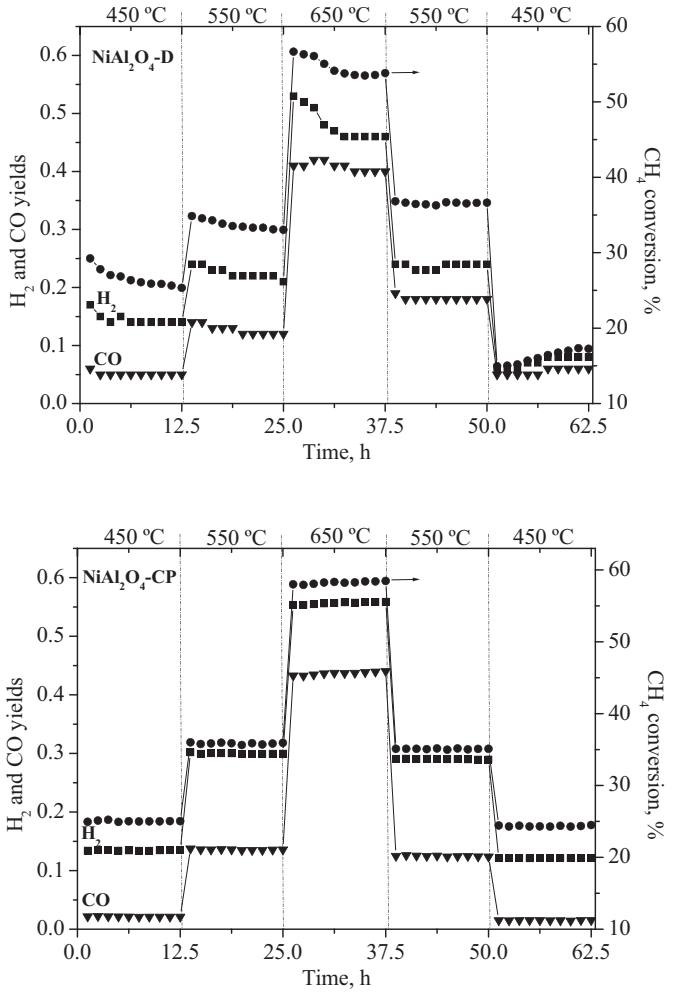

Fig. 9. Evolution of CH_4 conversion and H_2 and CO yield over the reduced *$NiAl_2O_4$-D and $NiAl_2O_4$-CP catalysts* with time on stream in POM reaction at 450, 550 and 650 °C. Reactions conditions: 38,400 cm^3 CH_4 g^{-1} h^{-1}; W = 0.125 g. Gas mixture: 10%CH_4/5%O_2/N_2.

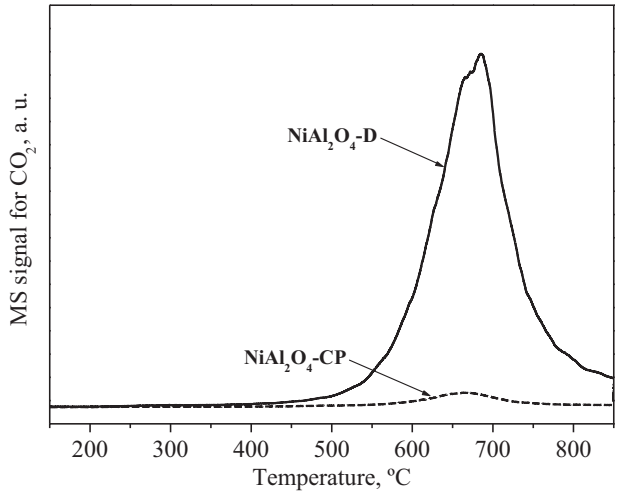

Fig. 10. TPO-MS analysis over spent $NiAl_2O_4$-D and $NiAl_2O_4$-CP catalysts after POM reaction.

NiO in our XRD diffractograms of the used samples could be justified. Furthermore, the presence of the NiO could explain the low CO/CO_2 ratios obtained at low temperatures suggesting that this gave rise to total oxidation instead of reforming reaction.

On the other hand, as described in previous works the carbon deposition may deactivate the catalyst either by covering of the active sites and/or by pore blocking [32,44–46]. In our case, it was found that, after catalytic tests, the pore size distribution of $NiAl_2O_4$-D catalyst shifted towards higher values (8.1–10.7 nm) suggesting the blocking of the pores with small sizes by carbon deposition (Table 1). In addition, it should be noted that carbon deposition on the $NiAl_2O_4$-CP and $NiAl_2O_4$-D catalysts appeared to significantly increase the surface area (Table 1). Thus, on $NiAl_2O_4$-D the specific surface area increased from 48 to 57 m^2 g^{-1} whereas over $NiAl_2O_4$-CP catalyst it increased from 55 to 64 m^2 g^{-1}, suggesting that this might be due to the similar porous nature of the carbon deposited on the two catalysts [46].

Moreover, the chemical properties of their near surface could have an effect on the catalytic activity and stability of $NiAl_2O_4$-D and $NiAl_2O_4$-CP catalysts. Generally, acidity is considered to induce a negative impact on methane reforming behaviour by catalysing the coke formation [32]. In agreement with our NH_3-TPD studies, the surface of $NiAl_2O_4$-D bears more acid sites than that of $NiAl_2O_4$-CP catalyst. This difference in the acid character could explain the markedly larger formation of coke on the surface of the $NiAl_2O_4$-D catalyst in comparison with $NiAl_2O_4$-CP.

In addition, the inversion degree of the formed spinel was another factor to take into consideration in order to explain the different performances of $NiAl_2O_4$-D and $NiAl_2O_4$-CP in POM reaction. In their study on the methane dry reforming reaction over nickel aluminate catalysts Kathiraser et al. [26] concluded that the inverse $NiAl_2O_4$ spinel structure positively affected the catalytic activity compared to the normal spinel. Our characterisation results showed that $NiAl_2O_4$-CP tended to be in the inverse coordination while the $NiAl_2O_4$-D was close to the normal spinel phase. The observed divergence between $NiAl_2O_4$-D and $NiAl_2O_4$-CP might influence the catalytic behaviour of these catalysts as well.

3.7.2. Steam reforming of methane (SRM)

Fig. 8 show CH_4 conversion and H_2, CO and CO_2 yields in the SRM reaction for the examined reduced catalysts as function of temperature. In all cases methane conversion as well as H_2, CO and CO_2 yields were stable with time on stream. Moreover, the $NiAl_2O_4$-CP and $NiAl_2O_4$-D catalysts were markedly more active than 1%Rh/Al_2O_3 (80% and 53% vs. 46% at 650 °C, respectively). The comparison of the performance of the $NiAl_2O_4$-D catalyst in POM and SRM reactions showed that replacing oxygen with steam resulted in poorer methane conversion and CO yield while it improved the H_2 production. By contrast, when compared to its performance in POM reaction, an increase in activity as well as CO and H_2 yields were observed over NiA_2O_4-CP catalyst in SRM reaction, especially at 550 °C and 650 °C. Furthermore, among the three catalysts the best methane conversion and the largest H_2, CO and CO_2 yields were achieved with $NiAl_2O_4$-CP at the three reaction temperatures. Thus, at 450 °C the $NiAl_2O_4$-D and 1%Rh/Al_2O_3 catalysts exhibited a poor performance as their activity did not exceed 10% (the $NiAl_2O_4$-CP catalyst gave a conversion of 21% at this temperature). It should be noted that the CO production, at 450 °C, was very low or negligible over the three tested catalysts. However, considerable yields of CO_2 (0.18 over $NiAl_2O_4$-CP and 0.07 over $NiAl_2O_4$-D) and H_2 (0.5 over $NiAl_2O_4$-CP and 0.22 over $NiAl_2O_4$-D) were obtained suggesting the main occurrence of water gas shift reaction. On the effect of the SRM reaction temperature on the catalytic performance of the Ni catalysts, we noted that higher temperatures improved conversion which rapidly increased to reach about 80% and 53% over $NiAl_2O_4$-CP and $NiAl_2O_4$-D, respectively (at

650 °C). Likewise, irrespective of the used catalyst both H_2 and CO yields increased as the SRM reaction temperature increased. This trend was more pronounced on the $NiAl_2O_4$-CP catalyst which led to CO (0.47 at 650 °C) and H_2 (1.6 at 650 °C) yields and a H_2/CO ratio close to the thermodynamic equilibrium.

On the other hand, as expected, the activity of the three catalysts was not accompanied by the carbon deposition (Table 3) which might be explained by adding water to the feed with a high H_2O/CH_4 ratio (around 3). The observed H_2/CO ratio was in all the cases higher than 6. As no significant carbon deposition was detected (Table 3), one could conclude that this was the reason for the stability of the $NiAl_2O_4$-D and $NiAl_2O_4$-CP tested catalysts. Note that, for both $NiAl_2O_4$-D and $NiAl_2O_4$-CP catalysts, no significant loss of their surface area was observed. XRD patterns of the $NiAl_2O_4$-D and $NiAl_2O_4$-CP catalysts recorded after the tests did not show any noticeable difference when compared with that of the freshly reduced samples suggesting that they did not undergo any noticeable alteration of their crystalline structures during the reaction (Fig. 2). However, an appreciable increase of Ni particle size was noticed in the case of $NiAl_2O_4$-D. Since this did not affect its catalytic stability the Ni particles growth was supposed to rapidly occur at the start of the reaction. Note that, while the stable catalytic behaviour could be eventually masked by mass transfer limitations at 650 °C, the fact is that a good stability was also noticed at lower temperatures (450 and 550 °C). In principle, the contribution of mass transfer limitations to the observed catalytic performance could be considered negligible under these conditions. In sum, it seems that the experimentally reforming behaviour of the $NiAl_2O_4$-D actually was that of a reduced spinel catalyst with a crystallite size of 47 nm (instead of 23 nm). This behaviour could be related with the nature of the Ni species deposited and their interactions with the carrier. Our characterisation results showed that the difference between the two $NiAl_2O_4$-CP and $NiAl_2O_4$-D catalysts was related to the fact that the reduction of the Ni species produced monodispersed fixed nickel on the first one whereas it produced larger particles of free nickel on the second one. On the effect of this distribution we could conclude, then, that the growth of Ni particles in SRM reaction, observed exclusively on $NiAl_2O_4$-D catalyst, concerned only the free deposited metallic Ni.

3.7.3. Oxidative steam reforming of methane (OSRM)

Finally the catalytic performance in OSRM reaction was also studied and the results are collected in Fig. 8. At the three investigated reaction temperatures the best methane conversion and the largest H_2 and CO yields, over the Ni catalysts, were achieved with the $NiAl_2O_4$-CP catalyst. Moreover, compared to its behaviour in POM reaction, a significant improvement of the catalytic activity could be noted; especially at 450 °C and 550 °C reaction temperatures where it was even more active than the 1%Rh/Al_2O_3 catalyst. By contrast, the $NiAl_2O_4$-D catalyst clearly gave the lowest methane conversion. Furthermore, the BET surface area of this sample decreased from 48 to 37 $m^2\,g^{-1}$ after reaction. Nevertheless, the water addition to the feed significantly improved the catalytic stability of $NiAl_2O_4$-D with respect to the POM reaction. Indeed, the literature reported that the excess of water or oxygen to the feed cleans the metallic surface and improve the stability of the catalyst [47]. Accordingly, our estimation of deposited coke, by thermogravimetric and TPO-MS analysis, was less than 1%wt. on both $NiAl_2O_4$-D and $NiAl_2O_4$-CP catalysts. On the other hand, the combination of POM and SRM gas mixtures seemed to increase the CO_2 yield, which attained 0.41 on the $NiAl_2O_4$-CP catalyst at 650 °C. Moreover, CO/CO_2 ratio did not exceed 0.5, which could be explained by a high combustion activity and a low reforming activity [10].

Fig. 2 also shows the XRD patterns of the $NiAl_2O_4$-D and $NiAl_2O_4$-CP catalysts used in OSRM reaction. The absence of 26.4° diffraction peak indicated that, on both catalysts, no graphite carbon deposition occurred during the tests. By contrast, changes in the Ni crystallite size were noted. For the $NiAl_2O_4$-D catalyst the Ni particle size increased from 22 up to 29 nm, whereas for the $NiAl_2O_4$-CP it decreased from 11 to 7 nm (Table 1). Similar changes were observed on the XRD patterns of the latter in POM reaction suggesting that a re-distribution of Ni active phases might have occurred which favoured its activity and stability. However, on the $NiAl_2O_4$-D catalyst this re-distribution (increased Ni particle size) provoked the decay of its activity. The XRD diffractograms of the used $NiAl_2O_4$-D and $NiAl_2O_4$-CP catalysts in OSRM reaction also showed the presence of intense diffraction peaks attributed to the NiO phase (Fig. 2). A similar behaviour was reported by Yoshida et al. [10] in their study of OSR reaction over Ni/α-Al_2O_3 and they explained it by the oxidation of the Ni species in the presence of gas-phase oxygen. The formation of these Ni oxidised species could explain the high activity of our Ni catalysts for methane combustion.

4. Conclusions

The behaviour of two bulk nickel aluminate ($NiAl_2O_4$-CP and $NiAl_2O_4$-D) has been investigated in the partial oxidation, steam reforming and oxidative steam reforming of methane. These catalysts have been prepared by co-precipitation and co-dissolution methods, respectively, and characterised by N_2 physisorption, XRD, UV–visible–NIR DRS, XPS, TEM, H_2-TPR and NH_3-TPD.

XRD, H_2-TPR, UV–visible spectroscopy and XPS analyses show that the two catalysts, calcined at 850 °C, contain nickel aluminate as a major phase together with NiO which was considered as an excess. Moreover, it has been proved that on the $NiAl_2O_4$-D catalyst nickel is preferentially hosted in tetrahedral sites of the inverse spinel whereas it tends to occupy the octahedral coordination in the case of $NiAl_2O_4$-CP sample. As showed by H_2-TPR, the interaction of the resulted NiO excess with the nickel aluminate seems to depend on the preparation method. Indeed, the reduction of this NiO excess on the $NiAl_2O_4$-D occurs at lower temperatures compared to the $NiAl_2O_4$-CP suggesting that on the latter NiO has a strong interaction with nickel aluminate. TEM results indicate that on the $NiAl_2O_4$-CP catalyst the reduction of the Ni species at 850 °C produces homogeneous and monodispersed fixed nickel whereas heterogeneous and larger metallic free nickel is detected on the $NiAl_2O_4$-D catalyst. In addition, this distribution has a marked effect on the chemical properties of the reduced catalysts since the surface of reduced $NiAl_2O_4$-D contains more acid sites than that of reduced $NiAl_2O_4$-CP.

A clearly different behaviour in the reforming of methane has been observed over the $NiAl_2O_4$-CP and $NiAl_2O_4$-D catalysts with same Ni composition but prepared by two different methods. The results show that the reforming efficiency is highly dependent on the type of interaction of the Ni active phase with the carrier. In the three tested reforming reactions the $NiAl_2O_4$-CP catalyst, prepared by co-precipitation method, has proved to be highly active and stable. However, as a result of the carbon deposition found in POM reaction, methane conversion, H_2, CO and CO_2 yields are not stable with time over the $NiAl_2O_4$-D catalyst. At low POM reaction temperatures (450 °C and 550 °C) CO disproportionation reaction occurs producing CO_2 and carbon. On the other hand, the H_2/CO ratio has resulted in all the cases higher than 2. By using steam instead of oxygen no significant carbon deposition has been detected on $NiAl_2O_4$-D catalyst, but it leads to lower methane conversion and CO yields while it improves the H_2 production. By contrast, it has been observed that this change of the composition of the reaction gas mixture is beneficial in the case of the $NiAl_2O_4$-CP catalyst. On both nickel aluminate catalysts the main

occurrence of water gas shift reaction at low temperature is evident. The combination of POM and SRM gas mixtures seems to increase the CO_2 yield and to decrease CO yields suggesting that there are high combustion activity and low reforming activity.

The performance differences, in the three assayed reactions, were related to the Ni particle size which played an important role in the catalytic activity of the two studied catalysts. Furthermore, concerning the behaviour of active metallic Ni species laying on the catalysts, the most important finding reported in this study is the remarkable stability of the reduced $NiAl_2O_4$-CP catalyst, which maintains its small Ni particle size during the reforming reactions. However, the presence of free metallic Ni (with larger size) on the $NiAl_2O_4$-D catalyst, which displayed an increase in its particle size, provokes a decay of its activity and stability.

Acknowledgements

The authors wish to thank the financial support for this work provided by the Spanish Science and Innovation Ministry (CTQ2010-16752), the Basque Government (PRE_2013_2_453, IT657-13) and the University of The Basque Country (UFI 11/39). Technical and human support from SGIker (XRD (A. Larrañaga), WDXRF (F.J. Sangüesa), XPS (M.B. Sánchez) and UV-vis-DRS (L.J. Bartolomé)) and CIC bioGUNE (D. Gil and S. Delgado) is also gratefully acknowledged.

References

[1] Y. Men, G. Kolb, R. Zapf, M. O'Connell, A. Ziogas, Appl. Catal. A 380 (2010) 15–20.
[2] P. Engelhardt, M. Maximini, F. Beckmann, M. Brenner, Int. J. Hydrogen Energy 37 (2012) 13470–13477.
[3] O. Pasdag, A. Kvasnicka, M. Steffen, A. Heinzel, Energy Proc. 28 (2012) 57–65.
[4] M. O'Connell, G. Kolb, K.P. Schelhaas, J. Schuerer, D. Tiemann, A. Ziogas, V. Hessel, Int. J. Hydrogen Energy 34 (2009) 6290–6303.
[5] J. Thormann, L. Maier, P. Pfeifer, U. Kunz, O. Deutschmann, K. Schubert, Int. J. Hydrogen Energy 34 (2009) 5108–5120.
[6] V.A. Tsipouriari, Z. Zhang, X.E. Verykios, J. Catal. 179 (1998) 283–291.
[7] P. Ferreira-Aparicio, M.J. Benito, J.L. Sanz, Catal. Rev. Sci. Eng. 47 (2005) 491–588.
[8] Y. Song, H. Liu, S. Liu, D. He, Energ. Fuel 23 (2009) 1925–1930.
[9] U.S. Amjad, A. Vita, C. Galletti, L. Pino, S. Specchia, Ind. Eng. Chem. Res. 52 (2013) 15428–15436.
[10] K. Yoshida, K. Okumura, T. Miyao, S. Naito, S. Ito, K. Kunimori, K. Tomishige, Appl. Catal. A 351 (2008) 217–225.
[11] Y. Wang, J. Peng, C. Zhou, Z. Lim, C. Wu, S. Ye, W.G. Wang, Int. J. Hydrogen Energy 39 (2014) 778–787.
[12] H. Özdemir, M.A.F. Öksüzömer, M.A. Gürkaynak, Int. J. Hydrogen Energy 35 (2010) 12147–12160.
[13] E. Acha, J. Requies, V.L. Barrio, J.F. Cambra, M.B. Güemez, P.L. Arias, Int. J. Hydrogen Energy 35 (2010) 11525–11532.
[14] R. López-Fonseca, C. Jiménez-González, B. de Rivas, J.I. Gutiérrez-Ortiz, Appl. Catal. A 437–438 (2012) 53–62.
[15] C. Jiménez-González, Z. Boukha, B. de Rivas, J.J. Delgado, M.A. Cauqui, J.R. González-Velasco, J.I. Gutiérrez-Ortiz, R. López-Fonseca, Appl. Catal. A 466 (2013) 9–20.
[16] I.E. Achouri, N. Abatzoglou, C. Fauteux-Lefebvre, N. Braidy, Catal. Today 207 (2013) 13–20.
[17] A. Ebshish, Z. Yaakob, B. Narayanan, A. Bshish, W.R. Daud, Energy Proc. 18 (2012) 552–559.
[18] Y. Bang, S.J. Han, J. Yoo, J.H. Choi, J.K. Lee, J.H. Song, J. Lee, I.K. Song, Appl. Catal. B 148–149 (2014) 269–280.
[19] J.H. Bitter, K. Seshan, J.A. Lercher, J. Catal. 183 (1999) 336–343.
[20] A.L. Pinheiro, A.N. Pinheiro, A. Valentini, J.M. Filho, F.F. de Sousa, J.R. de Sousa, M.G.C. Rocha, P. Bargiela, A.C. Oliveira, Catal. Commun. 11 (2009) 11–14.
[21] H.S. Bengaard, J.K. Nørskov, J. Sehested, B.S. Clausen, L.P. Nielsen, A.M. Molenbroek, J.R. Rostrup-Nielsen, J. Catal. 209 (2002) 365–384.
[22] J.R. Rostrup-Nielsen, Steam Reforming Catalysts, Danish Technical Press, Copenhagen, 1975.
[23] G. Li, L. Hu, J.M. Hill, Appl. Catal. A 301 (2006) 16–24.
[24] N. Salhi, A. Boulahouache, C. Petit, A. Kiennemann, C. Rabia, Int. J. Hydrogen Energy 36 (2011) 11433–11439.
[25] J.R.H. Ross, M.C.F. Steel, A.Z. Isfahani, J. Catal. 52 (1978) 280–290.
[26] Y. Kathiraser, W. Thitsartarn, K. Sutthiumporn, S. Kawi, J. Phys. Chem. C 117 (2013) 8120–8130.
[27] E.E. Kiss, G.C. Bošković, M.M. Lazić, G.A. Lomić, R.P. Marinković-Nedučin, React. Kinet. Catal. Lett. 88 (2006) 309–314.
[28] Y.S. Han, J.B. Li, X.S. Ning, X.Z. Yang, B. Chi, Mat. Sci. Eng. A 369 (2004) 241–244.
[29] R.F. Cooley, J.S. Reed, J. Am. Ceram. Soc. 58 (1972) 395–398.
[30] R. Subramanian, M. Higuchi, R. Dieckman, J. Cryst. Growth 143 (1994) 311–316.
[31] J.A. Peña, J. Herguido, C. Guimon, A. Monzon, J. Santamaría, J. Catal. 159 (1996) 313–322.
[32] C.H. Bartholomew, Appl. Catal. A 212 (2001) 17–60.
[33] P. Porta, A. Anichini, U. Bucciarelli, Faraday Trans. I 75 (1978) 1876–1887.
[34] J.N. Roelofsen, R.C. Peterson, Am. Mineral. 77 (1992) 522–528.
[35] H. Furuhashi, M. Inagaki, S. Naka, J. Inorg, Nucl. Chem. 35 (1973) 3009–3014.
[36] Z. Wang, C. Zhao, P. Yang, L. Winnubst, C. Chen, Solid State Ionics 177 (2006) 2191–2194.
[37] S.M. Patange, S.E. Shirsath, G.S. Jangam, K.S. Lohar, S.S. Jadhav, K.M. Jadhav, J. Appl. Phys. 109 (2011) 0539091–0539099.
[38] P. Kim, Y. Kim, H. Kim, I.K. Song, J. Yi, Appl. Catal. A 272 (2004) 157–166.
[39] H. Cai, G.C. Farrington, J. Electrochem. Soc. 139 (1992) 744–748.
[40] D.A. Hickman, L.D. Schmidt, J. Catal. 138 (1992) 267–282.
[41] V.R. Choudhary, T.V. Choudhary, Angew. Chem. Int. Ed. 47 (2008) 1828–1847.
[42] M.C. Campa, G. Ferraris, D. Gazzoli, I. Pettiti, D. Pietrogiacomi, Appl. Catal. B 142–143 (2013) 423–431.
[43] T. Bruno, A. Beretta, G. Groppi, M. Roderi, P. Forzatti, Catal. Today 99 (2005) 89–98.
[44] Z.L. Zhang, X.E. Verykios, Catal. Today 21 (1994) 589–595.
[45] R. Jin, Y. Chen, W. Li, W. Cui, Y. Ji, C. Yu, Y. Jiang, Appl. Catal. A 201 (2000) 71–80.
[46] S.Y. Foo, C.K. Cheng, T. Nguyen, E.M. Kennedy, B.Z. Dlugogorski, A.A. Adesina, Catal. Commun. 26 (2012) 183–188.
[47] S.M. Lima, A.M. Silva, L.O.O. Costa, U.M. Graham, G. Jacobs, B.H. Davis, L.V. Mattos, F.B. Noronha, J. Catal. 268 (2009) 268–281.